AD NUMBER
AD337278
CLASSIFICATION CHANGES
TO: unclassified
FROM: secret
LIMITATION CHANGES
TO: Approved for public release, distribution unlimited
FROM: Controlling Organization: British Embassy, 3100 Massachusetts Avenue, NW, Washington, DC 20008.
AUTHORITY
DSTL, AVIA 6/23869, 12 Feb 2009; DSTL, AVIA 6/23869, 12 Feb 2009

SECRET

AD 337 278

DEFENSE DOCUMENTATION CENTER

FOR

SCIENTIFIC AND TECHNICAL INFORMATION

CAMERON STATION, ALEXANDRIA, VIRGINIA

SECRET

ROYAL AIRCRAFT ESTABLISHMENT

(ABERPORTH)

TECHNICAL NOTE No. I.R. 13

THE USE OF LUNEBERG LENSES FOR RADAR ENHANCEMENT OF THE JINDIVIK TARGET AIRCRAFT [U]

by

J. E. A. Harrison

NOVEMBER, 1962

MINISTRY OF AVIATION

U.D.C. No. 535.317.1 : 621.396.963[A1](94) Jindivik

Technical Note No. I.R.13

November, 1962

ROYAL AIRCRAFT ESTABLISHMENT

(ABERPORTH)

THE USE OF LUNEBERG LENSES FOR RADAR ENHANCEMENT OF THE JINDIVIK TARGET AIRCRAFT

by

J. E. A. Harrison

SUMMARY

This note describes measurements of apparent radar glint and range performance made by using AI Mk.18 and AI Mk.23B radars against a Jindivik carrying various arrangements of Luneberg lenses. Although the results are few and statistically somewhat dissatisfying, they agree sufficiently closely with theory to make them worth while publishing.

Generally, a Luneberg lens of 20 sq. m. equivalent echoing area allows AI Mk.18 and AI Mk.23B radars to lock-on at about 20 miles, which is comparable with lock-on ranges achieved on Canberra aircraft viewed from dead astern.

The angle noise produced by two 12" lenses or a 10" and a 12" lens mounted on the wingtips of a Jindivik appears comparable with that produced by a Canberra at similar ranges.

LIST OF CONTENTS

LIST OF APPENDICES

LIST OF ILLUSTRATIONS

1 INTRODUCTION

The Jindivik target is small, and has a radar echoing area which varies with aspect between 0·5 and 2·0 sq. m. Most weapon systems and instrumentation radars require a larger echoing area, which must be provided by artificial enhancement. In the past, various methods of active enhancement have been used, such as transponder beacons and travelling wave amplifiers. All have worked successfully, but they have disadvantages (as have Luneberg lenses); the Luneberg lens overcomes many of the disadvantages of the transponder beacon, such as tuning and frequency stability.

This note describes some tests of range performance and glint using AI Mk.18 and AI Mk.23B radars to illuminate Luneberg lenses carried on Jindivik targets. The results are limited and should be treated with some caution, but appear to be consistent with theory.

2 PROPERTIES OF THE LUNEBERG LENS

The Concise Oxford English Dictionary defines a lens as "a lentil shaped glass with both sides (or one only) curved for concentrating or dispersing light rays". The Luneberg lens uses dielectric material to concentrate or disperse radio waves. The name is derived from the theoretical investigations of R. K. Luneberg[1] into the optical properties of such lenses, which first stimulated interest in their uses for microwave enhancement.

Luneberg lenses may be divided into two types, monostatic and bistatic. A monostatic lens theoretically radiates all the energy incident upon it back in the direction of incidence, whereas a bistatic lens reflects the energy back into a conical volume of space with its axis of symmetry lying along the direction of incidence. In practice, a perfect monostatic lens is impossible, partly because of the finite lens aperture and partly because of imperfections in the dielectric, and all lenses have some bistatic properties.

The Luneberg lens used for Jindivik enhancement is monostatic, and consists of a sphere of dielectric material with a metallic reflector covering some portion of the surface of the sphere.

The monostatic focussing properties of the spherical lens are obtained by varying the dielectric constant with the radius of the sphere. There are a large number of different relationships between dielectric constant and radius which will meet the requirement, and the general solution is quite involved[2], but the most common solution is

$$n = \sqrt{2 - \left(\frac{a}{r}\right)^2} \qquad (1)$$

where n = refractive index

a = radial distance $0 \leqslant a \leqslant r$

r = radius of sphere.

In practice a Luneberg lens is constructed of many thin spherical shells with progressive refractive indices, giving a stepped approximation to the relationship above.

A plane electromagnetic wave incident on a dielectric sphere constructed in this manner will be refracted and focussed to a point on the boundary of the spherical lens diametrically opposite to the point of entry of the wave. If a metallic reflector is placed at the focus point, the wave is reflected and emerges from an ideal lens as a plane wave reflected in the direction of incidence. Plane polarised waves are reflected with the same plane of polarisation, but circularly polarised waves are returned with their direction of rotation reversed, as from a flat plate.

The angular coverage of the Luneberg lens is controlled by the size of the reflector. Coverages up to a cone of semi-angle 70° are usable; greater angles can be achieved, but the return at large angles from the axis of symmetry of the lens is reduced because parts of the lens are obscured by the reflector.

So long as the aperture of a monostatic Luneberg lens is not obscured by the reflector, it can be regarded as a flat plate of effective area $A = \pi r^2$ which rotates to remain normal to the incident radiation. The echoing area of a flat plate at normal incidence is given by the formula

$$\sigma = \frac{4\pi A^2}{\lambda^2}$$

which is derived in many texts, e.g. Ref.3.

Then the theoretical echoing area of a monostatic Luneberg lens is given by

$$\sigma = \frac{4\pi A^2}{\lambda^2}$$

$$= \frac{4\pi^3 r^4}{\lambda^2} \qquad (2)$$

where σ = echoing area (sq. m.)

r = radius of lens (m.)

λ = wavelength of incident radiation (m.)

$A = \pi r^2$

It can be seen that the echoing area is inversely proportional to the square of the wavelength, so that a lens of given size provides much better enhancement at higher frequencies. In practice, because of lens imperfections and attenuation through the radome which must be used to protect the lens, this theoretical echoing area cannot be achieved.

Table 1 shows theoretical and practical echoing areas for 9", 10", 11" and 12" diameter lenses at three different frequencies: 8,500 Mc/s and 9,000 Mc/s are typical frequencies for AI radars; 5,500 Mc/s is a typical frequency for the AN/FPS.16 ground instrumentation radar.

3 ECHOING AREA REQUIRED FROM THE JINDIVIK TARGET

The echoing area required from the Jindivik target has been expressed in various ways at different times. These requirements are:

(a) area equivalent to 20 sq. m.,

(b) the same echo as that from a Canberra head-on or tail-on,

(c) adequate to ensure AI lock-on at a range of 15 nautical miles.

The relationship between the echoing area of a Luneberg lens, as defined by equation (2), and the echoing area of an aircraft is complex. Whereas a lens can be regarded as a simple target with no significant fluctuation in echoing area for small angular changes in the direction of viewing, an aircraft represents a multiple target with a considerable statistical fluctuation in echoing area. Measured echoing areas of jet aircraft normally follow a Rayleigh distribution, signifying that the target consists of a large number of elements reflecting waves whose relative phases are independent and vary randomly during the time of observation.

For simplicity in calculation, the echoing area is sometimes defined as the median value of a large number of observations of the echoing area. The cumulative properties of the Rayleigh distribution are shown in Fig.1, and compared with a simple distribution for a Luneberg lens of equivalent echoing area.

From Fig.1, it can be seen that although the detection range of an aircraft may be greater than the detection range of a Luneberg lens of equivalent echoing area, the lock-on range of an AI radar (which requires at least a 75 per cent probability of paint) on an aircraft is less than that for the lens because of the probability distribution. Expressed alternatively, comparing a non-fluctuating target with a fluctuating target of the same median echoing area, while the fluctuations degrade the performance at high probabilities (AI lock-on), they enhance the performance at long range (detection). See also Ref.4.

Having made these caveats, it now becomes possible to consider the experimental results obtained.

4 RESULTS OF EXPERIMENTAL TESTS ON AI DETECTION AND LOCK-ON RANGE

4.1 General experimental conditions

The target used for the detection and lock-on tests was a Jindivik pilotless aircraft carrying a 10" or 12" diameter Luneberg lens. The Jindivik was used because it has a very small natural echoing area; measurements show that its echoing area viewed from astern is about 0·5 sq. m. Thus glint or amplitude fluctuation effects caused by interference between the lenses and the natural echo should be small. Because the Jindivik is pilotless, and there is always a small but finite chance of losing it on any flight, the number of flights made was very limited. The results must therefore be approached cautiously.

The measurements were made by G.E.C. and Ferranti using AI Mk.18 and AI Mk.23B radars fitted to Canberra aircraft. Two methods of studying range performance were used. The first was to compare lock-on ranges of the radars on Canberra and enhanced Jindivik targets. The second was to measure AGC voltage versus range on the different types of target and to compare these.

The first method represented operational conditions but gave small samples of very poor statistical significance. The second method gave better samples but left the comparison between fluctuating and steady targets unresolved.

4.2 Detection measurements

The results from the first method are as follows:-

AI Mk.18 over sea (measurements by G.E.C. Ltd.)

Range for 75% detection of Canberra at 35,000 ft	= 25 n.miles
Range for 75% lock-on of Canberra at 35,000 ft	= 20 n.miles
Experimental results for detection of 10" dia. lens	= 27, 24 and 23 n.miles = 24·7 n.miles average
Experimental results for lock-on of 10" dia. lens	= 24, 23 and 16 n.miles = 21 n.miles average

AI Mk.23 over sea (measurements by Ferranti Ltd.)

Representative lock-on range on Canberra	= 19 n.miles
Experimental result for lock-on of 10" dia. lens	= 13 n.miles

(This was not a maximum range, but was limited by the flight pattern.)

AI Mk.23B over sea

Representative lock-on range on Canberra	= 22 n.miles
Experimental result for lock-on of 12" dia. lens	= 17 n.miles

(This was not a maximum range, but was limited by the flight pattern.)

4.3 AGC voltage measurements

AGC voltage measurements were made on Jindiviks equipped with four different lens combinations. They were:

(a) one 10" diameter lens

(b) one 12" diameter lens

(c) two 12" diameter lenses carried on the Jindivik wingtips (separation 19 ft approximately)

(d) one 10" and one 12" diameter lens carried on the Jindivik wingtips.

The results of the AI Mk.18 trials are plotted in Fig.2 and the AI Mk.23B results in Fig.3. They are again limited in number, and therefore of low statistical significance. Taking the Mk.18 results first, they appear to show that one 10" diameter lens is about equivalent to the rear view of a Canberra at equal altitude, while the two lens combinations (one 10" and one 12" or two 12") are approximately 4-5 dB greater.

The Mk.23B results are more complex. There is firstly an apparent difference between the echoing areas of the Canberra viewed tail-on at equal altitude and viewed from below, the area at equal altitude being lower.

Secondly, there are signs that the calibration of the AGC voltage is slightly non-linear, giving results differing from the R^{-4} law which one would expect.

The conclusions are generally in accord with the AI Mk.18 conclusions. That is, that a single 12" lens is about 3-4 dB better than a Canberra at equal altitude. The lens combinations are approximately equal, and about 4-5 dB higher than the single lens.

It must be emphasised once again that the results are of limited statistical significance, and many more results would be needed before final conclusions could be reached. However, they do show that Luneberg lenses of 20 and 40 sq. m. equivalent echoing area provide the same order of signal as a Canberra viewed tail-on at equal altitude, and that either lens combination will give a range performance greater than that on the Canberra.

5 GLINT EFFECTS

5.1 Theoretical considerations

If a number of lenses are used to give radar enhancement when the target is viewed from any angle, it is inevitable either that gaps will exist between the lens polar diagrams or that at some angles, two lenses will be visible to the illuminating radar at the same time. If the signals returned from the two lenses have similar amplitudes, when they are approximately in anti-phase at the radar receiver a distorted combined phase front is produced which shifts the apparent origin of the combined signal outside the line joining the two lenses. Since the two signals are of similar amplitude and nearly in anti-phase, the combined signal is very small and, due to the natural oscillations of the target, the anti-phase relationship only lasts for a very short time. However, if the two lenses are mounted on the wingtips, the apparent origin of the combined signal may move several wing spans outside the target, causing a large transient error signal.

Fortunately, because the glint error is transient, its effect on the radar is greatly reduced by smoothing introduced by the AGC and servo time constants of the radar.

The theory of angular glint is derived in Appendix 1 and also in Refs.5 and 6. The angular error due to glint can be expressed as:-

$$\theta_o = \theta_D \frac{1 - a^2}{1 + 2a \cos \phi + a^2} \qquad \text{(3 and A.12)}$$

where θ_o = angular error

$2\theta_D$ = apparent angular separation between two lenses

a = ratio of signal amplitude from two lenses

ϕ = phase difference between two signals at radar

When ϕ approaches 180° and a approaches 1, the angular error can be very large. The theoretical glint for various values of ϕ and a is shown in Fig.5.

It can be seen from Fig.5 that when a approaches 1, the glint spikes are very large, but only extend over a small range of ϕ. When a is smaller, the glint spikes are smaller but extend over a wider range of phase difference, ϕ.

A description in more physical terms is given below. Consider first a target B on axis (Fig.6a). Then the signals received by the upper and lower beams are equal and, after subtraction, the error signal is zero. For a target A above the axis, the signal received by the upper beam is greater than that received by the lower beam, and the radar must move upwards to reduce the error to zero.

In Fig.6b, we have a two element target AB with the larger element B on axis. Let the phase angle between reflections from the two elements be ϕ, and let the signals from the two target elements be represented by voltage vectors $\bar{E}_A$ and $\bar{E}_B$, and let $\bar{E}_B = 2\bar{E}_A$.

When the phase angle ϕ is small, the resultant signal amplitudes received in the upper and lower beams are shown in Fig.6c. $\bar{E}_{AU}$ is greater than $\bar{E}_{AL}$ because A is nearer the axis of the upper beam, while B is on the boresight axis, giving equal signals in both beams. The resultant in the upper beam is therefore greatest and the aerial moves up.

When ϕ is large, conditions are shown in Fig.6(d). Although $\bar{E}_{AU}$ is still greater than $\bar{E}_{AL}$, it can be seen that the resultant signal is now greater in the lower beam, giving a signal driving the aerial down and outside the linear dimensions of the target.

Both the discussions above refer to a monopulse radar as tracker, but substantially the same arguments can be applied to a conically scanning radar.

5.2 Experimental results

Although the theory of glint is simple, the practical amplitudes to be expected from a Jindivik equipped with two lenses in pods were unknown. We therefore decided to try to simulate the worst possible glint conditions in two ways. Both used two lenses carried on the wingtips of a Jindivik 102.

The first installation had two 12" diameter 140° lenses pointing dead astern, so that their covers overlapped. This was expected to give very narrow but large dips in received signal strength, each accompanied by a large shift of apparent signal origin (a approaching 1).

The second installation had a 12" diameter lens in one pod, and a 10" diameter lens in the other. Here the signal fades should be smaller but should last longer (a approximately 0·5). In a system containing time constants, there was a possibility that this installation might cause more glint than the sharp dips caused by two equal lenses.

5.2.1 AI Mk.18 results

Because of shortage of time, the instrumentation system in the aircraft was used as it stood. A 14-channel galvanometer recorder and a Pilot Attack Sight (PAS) Recorder were used to obtain continuous records, while measurements of AGC levels were recorded by the observer at known ranges.

The 14-channel recorder was used to measure:-

(a) Azimuth sight line error

(b) Elevation sight line error

(c) Signal level

(d) Range marks every 2,000 yards.

No detailed analysis of the azimuth or elevation errors has been made. However, the errors with all the lens arrangements appear to be comparable with those measured from a Canberra at the same range. The single 10" lens appeared a steadier target on the PPI than the Canberra. With the multiple lens arrangements, there were periods when the apparent radar centre of the target was moving $\pm 0 \cdot 25^\circ$ at about 3 c/s. These periods of glint lasted for about 3-8 seconds, and compare with expected errors from a Canberra of $\pm 0 \cdot 23^\circ$ in azimuth and $\pm 0 \cdot 1^\circ$ in elevation at comparable ranges.

5.2.2 AI Mk.23B results

The AI Mk.23B results were obtained using an instrumented Canberra operated by Ferranti Ltd., Edinburgh. Here again, we had a camera photographing the Pilot Attack Sight, together with a 16 channel galvanometer recorder measuring, amongst other parameters:

(a) Range voltage

(b) AGC voltage

(c) Radar azimuth error monitor

(d) Radar elevation error monitor

(e) Sight line spin Azimuth

(f) Sight line spin Elevation

(g) Scanner angle Azimuth

(h) Scanner angle Elevation

(j) Time

We will now consider some of these parameters in turn.

AGC voltage

The single lens showed few fades, and those which did occur tended to be slight. The fade pattern from the asymmetrical lens system appeared very similar to that from a Canberra, consisting of slow fades of up to 24 dB, lasting for about 1 second.

The symmetrical lens fade pattern was more interesting. At long range (>50,000 ft) the AGC voltage was oscillating at about 11 c/s, but from 50,000 ft inwards there were short deep fades, shorter and deeper than those normally experienced with a Canberra target. The frequency of fading decreased as the range decreased; thus between 50,000 and 40,000 ft there were 31 fades in 34 seconds, while between 30,000 and 20,000 ft there were 12 fades in 30 seconds. At shorter ranges there were very few fades. The average duration of fades was about 0·2 seconds, compared with fades longer than 1 second for the Canberra. No satisfactory explanation has been found for the very rapid oscillations at long range.

Angle tracking channels

The noise produced in these channels by both twin lens systems was very similar to that produced by a Canberra, except that, at ranges less than 10,000 ft, the noise produced by the Canberra was greater.

For the single lens, elevation noise remained similar to that from a Canberra, but the azimuth noise was lower.

Ranging servos

There appeared to be no significant differences in the noise on the long and short range rate outputs for the different targets.

6 CONCLUSIONS

6.1 Glint

Although the AGC recordings from both AI Mk.18 and AI Mk.23B show that sharp amplitude fades occur with a double lens system, the tracking errors produced appear to be no worse than those experienced when tracking a Canberra target. It is interesting to note that the distance between the Canberra engines is very nearly the same as the distance between the two lenses on the Jindivik wingtips.

When a single lens is used, elevation errors remain similar to those from a Canberra, but azimuth errors are somewhat reduced.

6.2 Range performance

A 10" lens in a hemispherical radome has an echoing area of between 18 and 20 sq. m. at the operating frequencies of the AI radars. An 11" lens is 1·6 dB greater and a 12" lens is 3 dB greater. The median echo from a double 12" lens system is a further 3 dB greater, i.e. 6 dB above a 10" lens.

Thus the final conclusions are:

(a) a 10" lens with a hemispherical radome (effective echoing area between 18 and 20 sq. m.) is equivalent to a Canberra at equal height viewed from the tail,

(b) a 12" lens with a hemispherical radome is about 3-4 dB greater than a Canberra,

(c) a two 12" lens system generally shows results about 6 dB higher than those from a Canberra,

(d) a single lens system will give a shorter pick-up range but a longer lock-on range than that from an aircraft target of equivalent echoing area,

(e) a two lens system should give pick-up and lock-on ranges similar to those from an aircraft target of equivalent echoing area.

7 RECOMMENDATIONS

The results are very limited, and all trials should be repeated to give a better statistical basis. In particular, the acquisition and lock-on ranges of the AI Mk.23B against various lens arrangements should be measured directly at long ranges.

8 ACKNOWLEDGMENTS

The work of G.E.C. Ltd. and Ferranti Ltd. in carrying out the trials and analysing the results is gratefully acknowledged. They are, however, in no way responsible for the conclusions drawn.

LIST OF REFERENCES

No.	Author	Title, etc.
1	Luneberg, R.K.	Mathematical theory of optics. Brown University Press, pp.189-212. 1944.
2	Morgan, S.P.	General solution of the Luneberg lens problem. Journal of Applied Physics. pp.1358-1368. September 1958.
3	Ridenour, L.N.	Radar system engineering. Vol.1. Radiation Lab. Series, McGraw Hill, pp.64-68, 78, 80. 1947.
4	Raven, R.S.	Airborne radar. Chapter 3, Van Nostrand, 1962.
5	Meade, J.	Guidance. ed. A.S. Locke. Van Nostrand, pp.440-442.
6	Hammond, P.H.	Amplitude and glint fluctuations due to a target comprising discrete point sources rigidly mounted in line. R.R.E. Memo No.1451. October 1958.
7	Smith, R.A.	The relative advantages of coherent and incoherent detectors: a study of their output noise spectra under various conditions. Proc. I.E.E. Vol.98, Part IV, pp.43-54.

ATTACHED:-

Appendices 1 and 2
Table 1
Drg. Nos. IR/P 120-124, 146
Detachable Abstract Cards

ADVANCE DISTRIBUTION:-

M.O.A. Headquarters

DG/GW
GW(G&C)5 12
TIL1(b) 150

Other addressees

WRE (Mr. Gibson, T.A. Group)
RRE (Mr. Milnes, Airborne Radar)
GEC Ltd., Pershore (Mr. Bailey)
GEC Ltd., Stanmore
Ferranti Ltd., Edinburgh (Mr. Holmes)

R.A.E.

Director
DD(E)
DD(A)
Pats 1(b)
Head of I & R Dept
Head of Radio Dept
Head of Weapons Dept
Library
Supt Aberporth
Officer i/c West Freugh
Officer i/c Llanbedr
Officer i/c Larkhill

APPENDIX 1

THE EFFECT OF GLINT ON THE ANGULAR ACCURACY OF A MONOPULSE OR STATIC-SPLIT RADAR

A monopulse or static-split radar is a narrow-beam tracking radar which measures the range of a target and its angular deviation from the centre of the radar beam every time a pulse returns to the radar.

The monopulse aerial system can measure angle either by amplitude or phase comparison of signals in different parts of the aerial system. For amplitude comparison a parabolic reflector is used, fed by four horns. In transmit, all four horns radiate simultaneously and produce a polar diagram which is symmetrical about the aerial axis. In receive, the signals from the four horns are added and subtracted (either in a microwave network or after rectification) to produce signals related to the angular deviation of the target from the radar axis.

For phase comparison, separate parabolic reflectors are used for each receiving beam. As examples, the AN/FPS.16 precision radar uses amplitude comparison, while the AI Mk.23B uses phase comparison for lateral angle measurement and amplitude comparison for vertical measurement.

Although the analysis below applies to an amplitude comparison system, similar results can be obtained for phase comparison and conically-scanning systems.

Let us first consider the way in which the error signal for a single point target is derived. The aerial receive polar diagram in the vertical plane is as represented in Fig.4. Let us assume that the crossover line between the upper and lower lobes provides the angle datum, and that a single point target is at an angle θ_o from this datum. If θ_o is small, we can assume that the received signal is a linear function of the error angle.

If the target is above the crossover point, the RF voltage received by the upper lobe can be expressed as:-

$$E_u = G[1+p\theta_o] \cos 2\pi f_o t \qquad (A.1)$$

and by the lower lobe as:-

$$E_L = G[1-p\theta_o] \cos 2\pi f_o t \qquad (A.2)$$

where G is a factor lumping together target size, system gain, range, etc., f_o is the carrier frequency, and p is the slope of the error polar diagram.

The signals from the two lobes are added and subtracted in a microwave network. The difference signal between the two lobes is a measure of the error, and after frequency conversion to intermediate frequency (IF), it is fed through amplifiers whose gain is controlled by the amplitude of the sum signal using Instantaneous Automatic Gain Control (IAGC). The IAGC voltage operates to maintain the amplitude of the difference signal for a given angular error the same as far as possible, thereby keeping the gain of the angle error detection loop sensibly constant.

To remove the IF carrier and derive a signal directly proportional to error, the IF error signal is fed to a phase sensitive detector, together with the reference signal also transposed to IF. The action of a phase sensitive detector is discussed further in Appendix 2; it can be regarded as a multiplicative detector with a difference input

$$\begin{aligned} E_D &= E_u - E_L \\ &= 2G_1\, p\theta_o \cos 2\pi f_1 t \end{aligned} \qquad (A.3)$$

and a sum input (see Appendix 2)

$$E_s = \frac{4}{\pi} \cos 2\pi f_1 t \qquad (A.4)$$

where f_1 = IF frequency

G_1 = lumped factor at output of IF amplifier.

The output error signal is:-

$$\begin{aligned} i &= \frac{8}{\pi} G_1\, p\theta_o \cos^2 2\pi f_1 t \\ &= \frac{8}{\pi} G_1\, p\theta_o\, (1 + \cos 4\pi f_1 t) \end{aligned}$$

and, since high frequency terms are rejected by filtering, we can write:-

$$i = \frac{8}{\pi} G_1\, p\theta_o\, . \qquad (A.5)$$

When the radar is pointing at the target, $\theta_o = 0$ and $i = 0$.

Let us now consider a target consisting of two elements, A and B (Fig.4). Each element contributes to the received signal, and the returned signals from each element have the same frequency, but a phase difference proportional to the range difference from the radar.

Let θ_o = angle between crossover line and centre of target

$2\theta_D$ = angular width of target as seen from radar

$a = \frac{E_B}{E_A}$ = ratio of returned signals from two elements

$\omega_o = 2\pi f_o$ = angular carrier frequency

$\omega_1 = 2\pi f_1$ = angular IF frequency.

Then we can write for the lobe voltages:-

$$E_u = G\left[1 + p(\theta_o - \theta_D)\right] \cos \omega_o t + aG\left[1 + p(\theta_o + \theta_D)\right] \cos(\omega_o t + \phi) \quad \ldots (A.6)$$

$$E_L = G\left[1 - p(\theta_o - \theta_D)\right] \cos \omega_o t + aG\left[1 - p(\theta_o + \theta_D)\right] \cos(\omega_o t + \phi). \quad \ldots (A.7)$$

Following the procedure for the single element:-

$$E_s = \frac{4}{\pi}\left[\cos \omega_1 t + a \cos(\omega_1 t + \phi)\right] \quad (A.8)$$

$$E_D = 2G_1 p\left[(\theta_o - \theta_D) \cos \omega_1 t + a(\theta_o + \theta_D) \cos(\omega_1 t + \phi)\right] \quad (A.9)$$

and the output of the phase sensitive detector is:-

$$\begin{aligned} i = \frac{8}{\pi} G_1 p \Big[&(\theta_o - \theta_D) \cos^2 \omega_1 t + a(\theta_o + \theta_D) \cos \omega_1 t \cos(\omega_1 t + \phi) \\ &+ a(\theta_o - \theta_D) \cos \omega_1 t \cos(\omega_1 t + \phi) \\ &+ a^2(\theta_o + \theta_D) \cos^2(\omega_1 t + \phi)\Big]. \end{aligned} \quad (A.10)$$

Rejecting higher frequency elements by a low pass filter as before:-

$$\begin{aligned} i &= \frac{8}{\pi} G_1 p\left[(\theta_o - \theta_D) + a(\theta_o + \theta_D) \cos \phi + a(\theta_o - \theta_D) \cos \phi + a^2(\theta_o + \theta_D)\right] \\ &= \frac{8}{\pi} G_1 p\left[\theta_o(1 + 2a \cos \phi + a^2) + \theta_D(a^2 - 1)\right]. \end{aligned} \quad (A.11)$$

The radar will move to make $i = 0$. The condition for this is:-

$$\theta_o = \theta_D \frac{1 - a^2}{1 + 2a \cos \phi + a^2}. \quad (A.12)$$

APPENDIX 2

THE PHASE SENSITIVE DETECTOR

The theory of a phase sensitive detector is discussed fully in Ref.7. A brief summary is as follows:-

In the phase sensitive detector, the polarity of the output of an amplifier is reversed at regular intervals corresponding to a half-cycle of the sinusoidal signal to be observed.

The action of the detector may be represented by multiplying the input by a function ψ which is the well-known "square-wave" function. Thus (neglecting noise)

$$i = (E \cos 2\pi ft)\, \psi(2\pi ft + \alpha) \tag{A.13}$$

where i = output current

E = amplitude of sinusoid being detected

f = frequency of sinusoid

α = phase difference between input and switching signals

and the function $\psi(x)$ is defined as follows:

$$\left.\begin{aligned} \psi(x) &= 1 \qquad -\frac{\pi}{2} \leq x < \frac{\pi}{2} \\ &= -1 \qquad \frac{\pi}{2} \leq x < \frac{3\pi}{2} \end{aligned}\right\} \tag{A.14}$$

For other values of x, ψ is defined by the condition that it is periodic with period 2π.

The function $\psi(x)$ can be expanded as a cosine Fourier series (being an even function of x) in the form

$$\psi(x) = \frac{4}{\pi}\left[\cos x - \frac{1}{3}\cos 3x + \frac{1}{5}\cos 5x - \dots\right]. \tag{A.15}$$

The current i in the output may therefore be expressed in the form

$$i = \frac{4}{\pi} E \cos 2\pi ft \left[\cos(2\pi ft + \alpha) - \frac{1}{3}\cos(6\pi ft + 3\alpha) + \frac{1}{5}\cos(10\pi ft + 5\alpha)\right]. \tag{A.16}$$

Only the first term in the expansion of the series for $\psi(x)$ need be considered, as the others are removed by a low-pass filter.

In the particular phase sensitive detector considered in Appendix 1, $\alpha = 0$.

We can therefore treat the phase sensitive detector as a multiplicative detector in which the input signal is multiplied by a reference sine wave of amplitude $4/\pi$ at the fundamental frequency.

TABLE 1

Theoretical and practical echoing areas for various lenses and radomes

Lens diameter	Frequency - 9,000 Mc/s			Frequency - 8,500 Mc/s			Frequency - 5,500 Mc/s		
	theory sq.m.	hemispherical radome - sq.m.	conical radome - sq.m.	theory sq.m.	hemispherical radome - sq.m.	conical radome - sq.m.	theory sq.m.	hemispherical radome - sq.m.	conical radome - sq.m.
9 ins.	19·8	13·8	7·9	17·7	12·4	7·1	7·5	5·25	3·0
10 ins.	28·8	20·2	11·5	25·7	18·0	10·3	10·8	7·6	4·3
11 ins.	42·3	29·6	16·9	37·7	26·4	15·1	15·9	11·1	6·7
12 ins.	60·0	42·0	24·0	53·5	37·5	20·4	22·6	15·8	9·1

Figures based on measurements by Fairey Eng. Ltd.

25% loss for practical lens

5% loss for hemispherical radome (both ways)

35% loss for conical radome (worst case both ways)

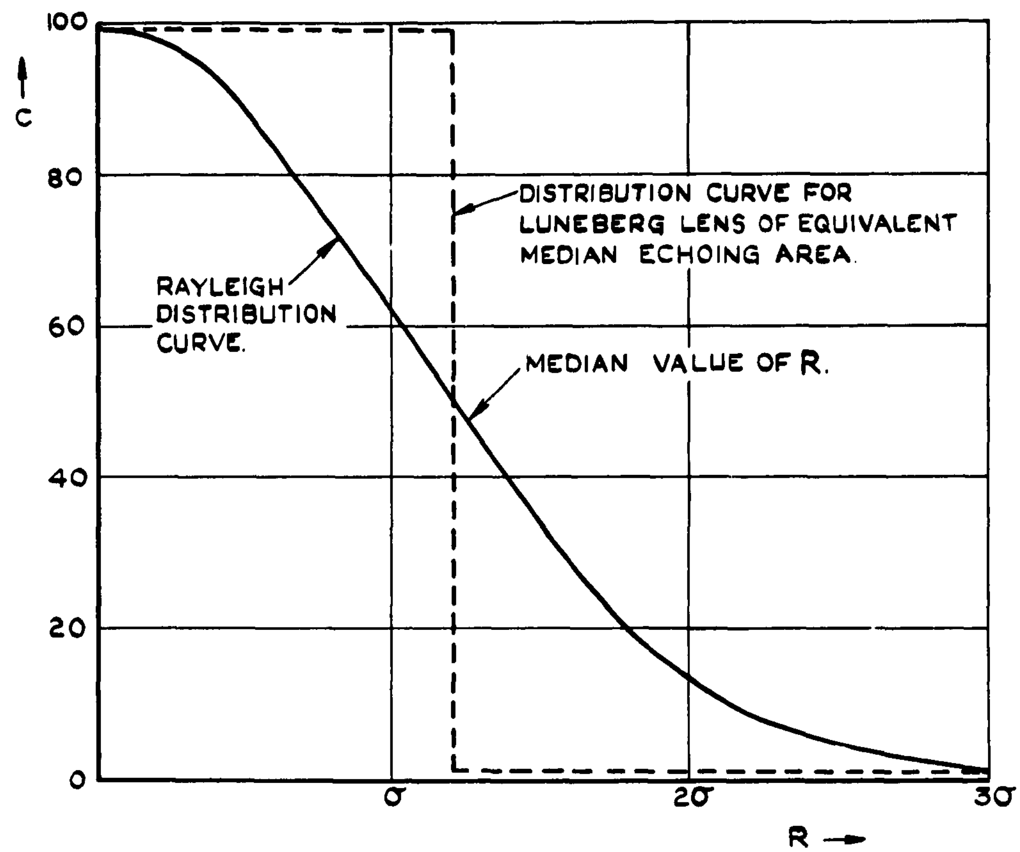

DISTRIBUTION IS DEFINED BY $p(R) = \frac{R}{2\sigma^2} e^{\frac{-R^2}{2\sigma^2}}$

WHERE R = MAGNITUDE OF VECTOR SUM OF THE PHASORS.
σ = STANDARD DEVIATION OF ONE COMPONENT OF THE BIVARATE DISTRIBUTION.
C = PROBABILITY IN PERCENTAGE THAT R EXCEEDS VALUE ON THE R AXIS.

FIG. 1. CUMULATIVE PROBABILITY DISTRIBUTION FOR AIRCRAFT ECHOING AREA (RAYLEIGH DISTRIBUTION) AND FOR LUNEBERG LENS ON SAME MEDIAN ECHOING AREA.

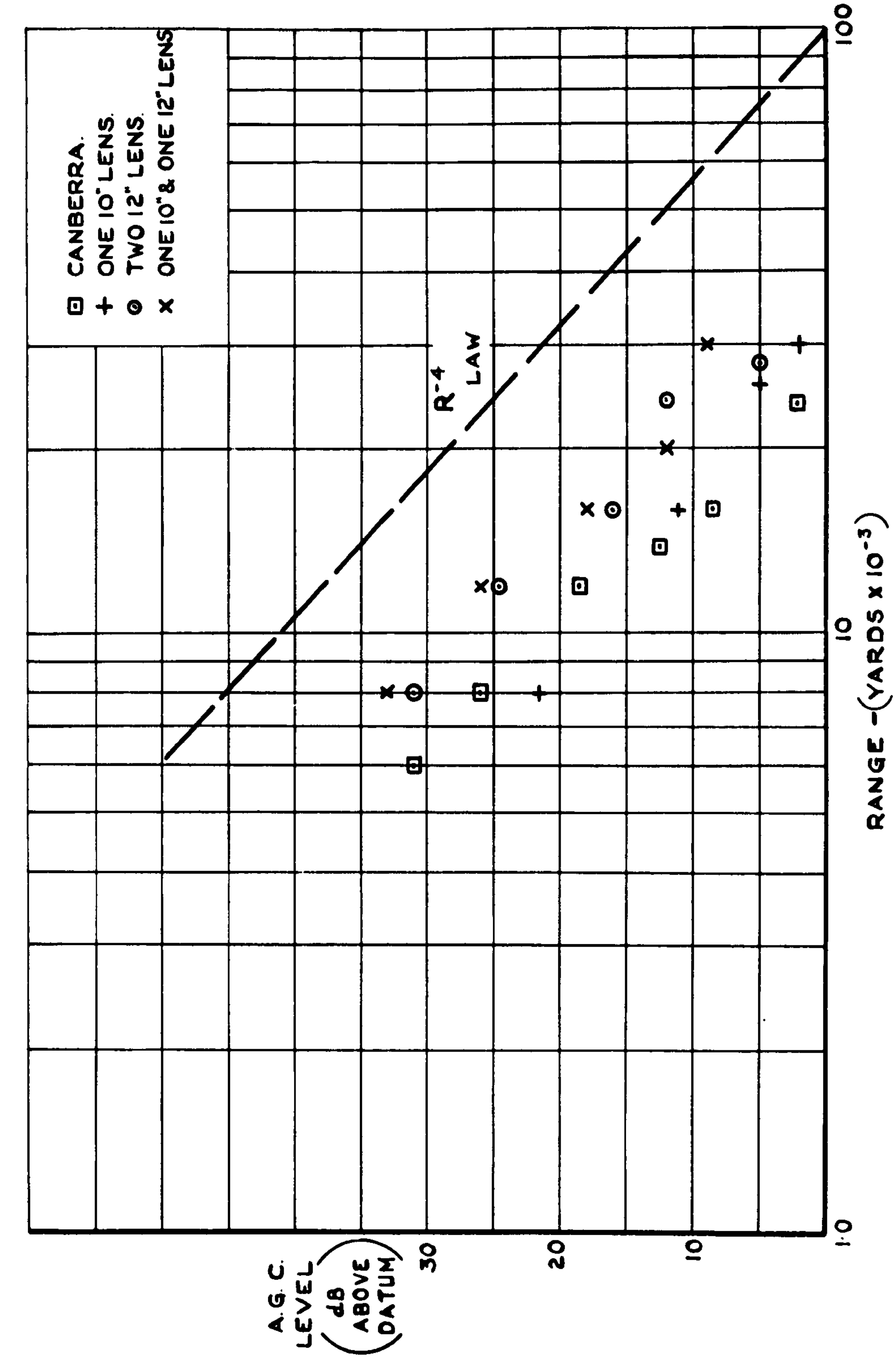

FIG. 2. A.G.C. VOLTAGE MEASUREMENTS USING AI. MK. 18.

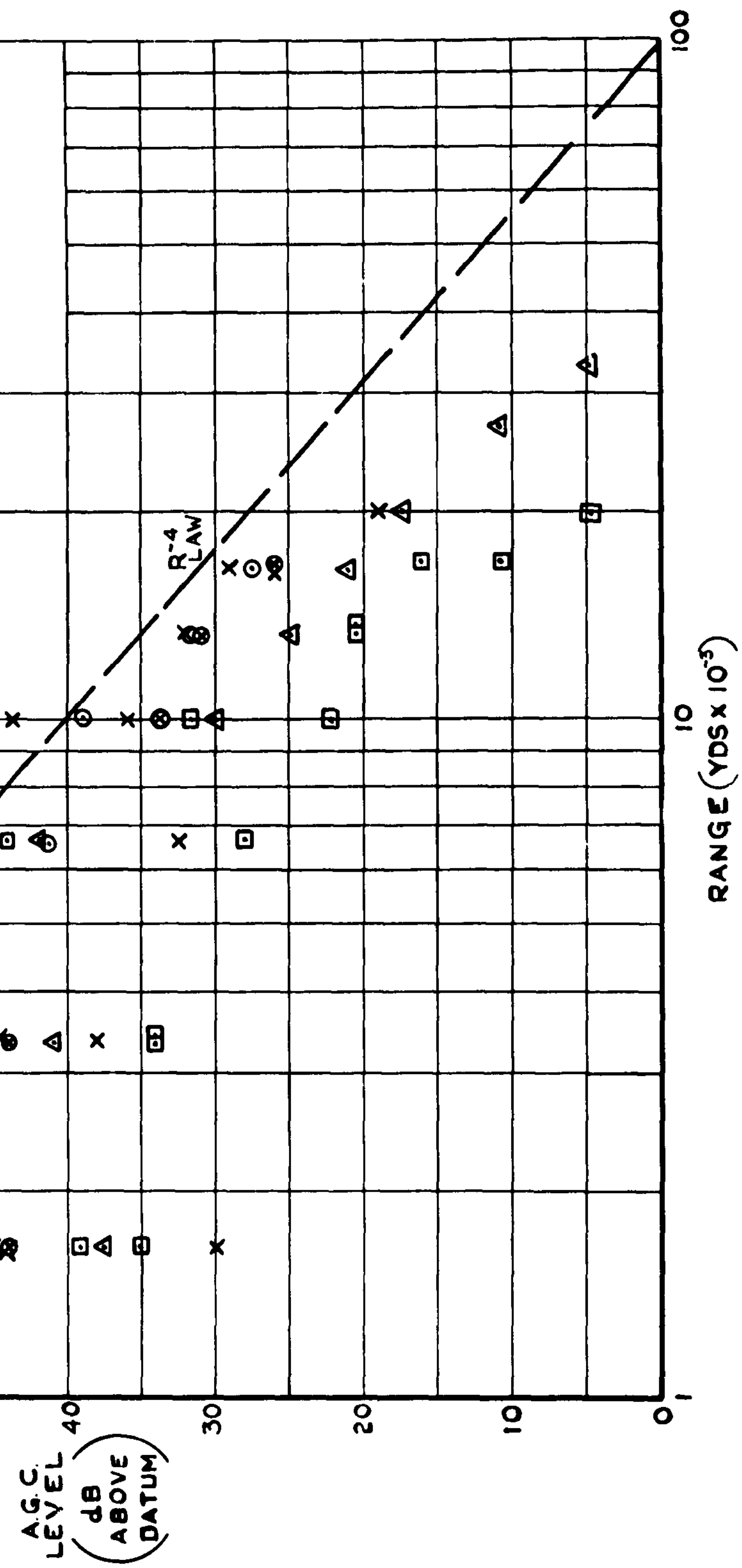

FIG. 3. A.G.C. VOLTAGE MEASUREMENTS USING AI. MK. 23B.

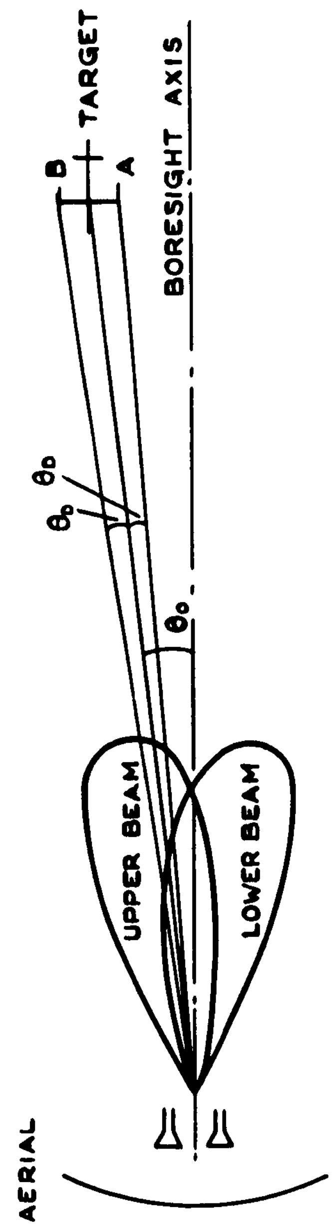

FIG. 4. SYMBOL CONVENTIONS FOR GLINT DISCUSSION.

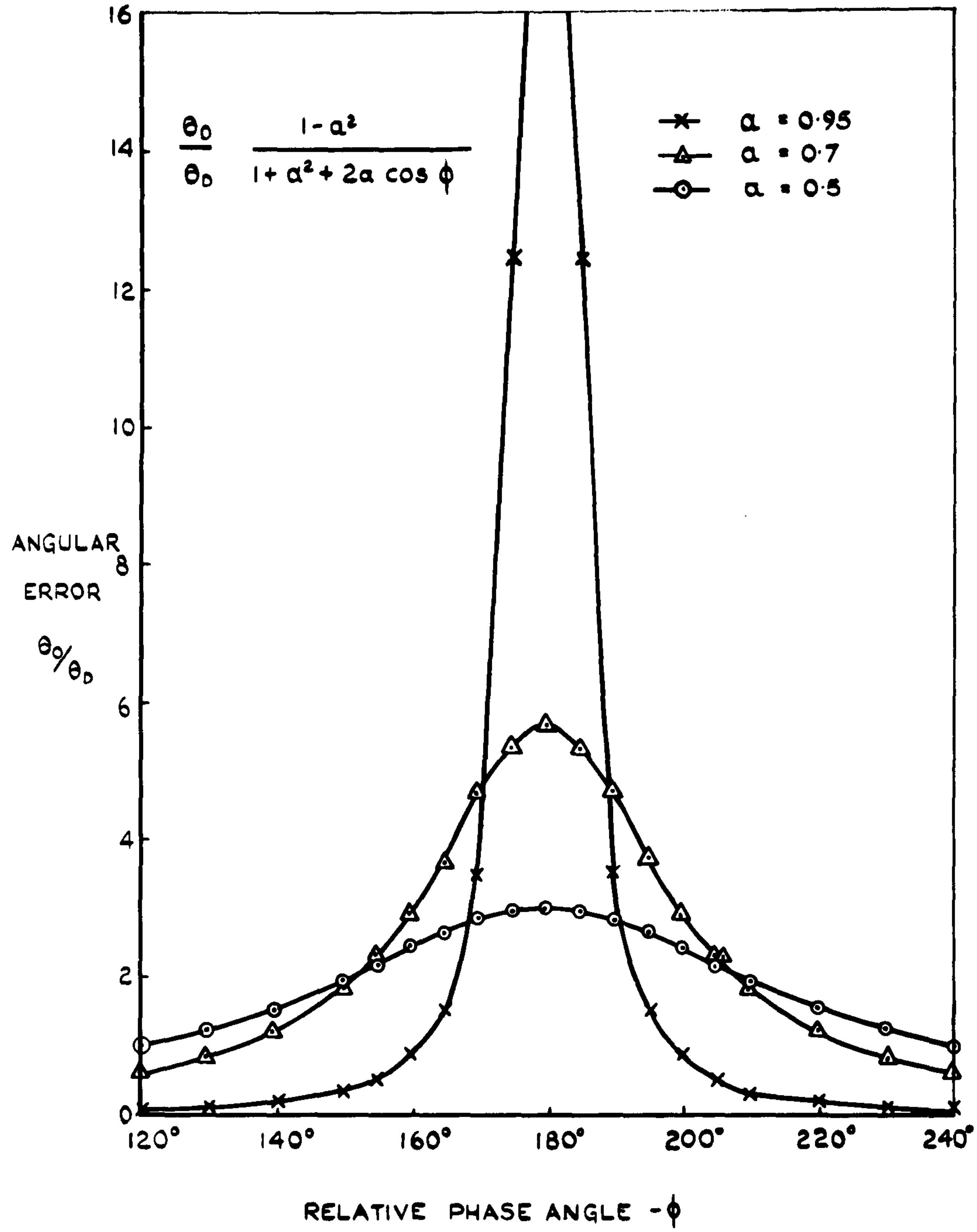

a = AMPLITUDE RATIO
θ_0 = ANGULAR ERROR
$2\theta_D$ = ANGULAR SEPARATION BETWEEN SOURCES.

FIG. 5. VARIATION OF ANGULAR GLINT WITH RELATIVE PHASE ANGLE FOR SELECTED RATIOS OF SOURCE AMPLITUDES.

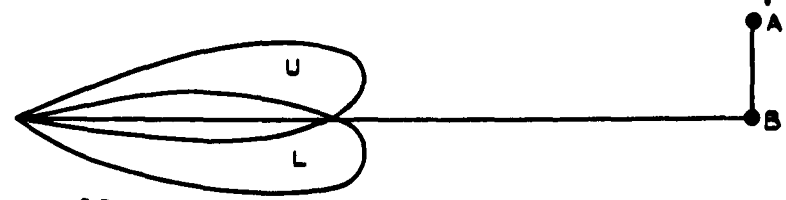

(a) DIAGRAMMATIC REPRESENTATION OF TARGET.

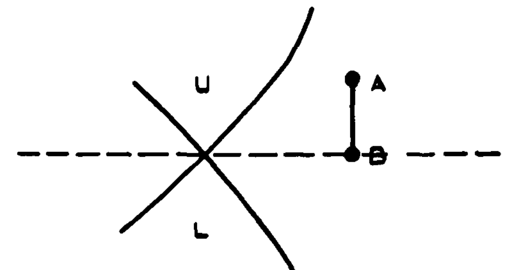

(b) EXPANSION OF (a) ABOVE.

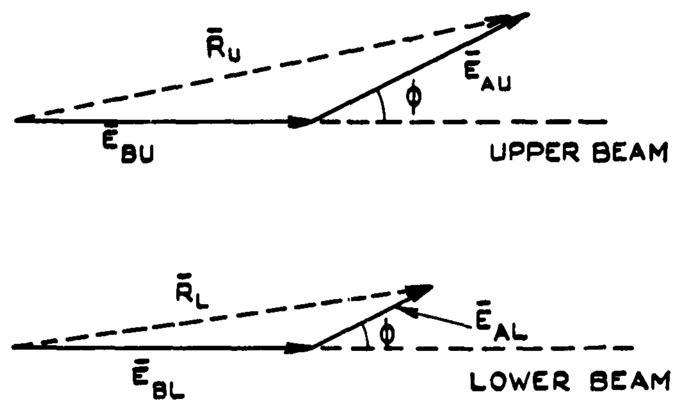

$\bar{R}_U > \bar{R}_L$ WHEN $\bar{E}_{AU} > \bar{E}_{AL}$

(c) VECTOR DIAGRAMS, ϕ SMALL.

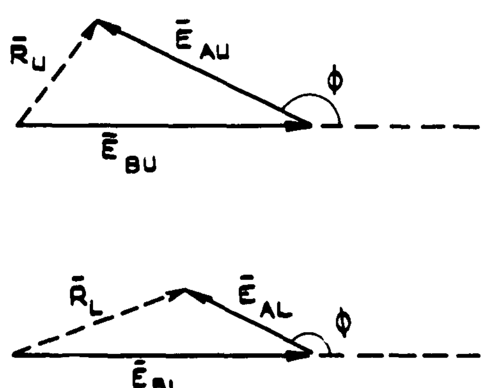

$\bar{R}_U < \bar{R}_L$ WHEN

$\bar{E}_{AU} > \bar{E}_{AL}$.

(d) VECTOR DIAGRAMS, ϕ LARGE.

FIG. 6. DIAGRAMMATIC REPRESENTATION OF GLINT.

DETACHABLE ABSTRACT CARDS

These abstract cards are inserted in Reports and Technical Notes for the convenience of Librarians and others who need to maintain an Information Index.

Detached cards are subject to the same Security Regulations as the parent document, and a record of their location should be made on the inside of the back cover of the parent document.

SECRET

Technical Note No. I.R.13
Royal Aircraft Establishment, Aberporth

535.317.1:
621.396.963[A1](94)
Jindivik

THE USE OF LUNEBERG LENSES FOR RADAR ENHANCEMENT OF THE JINDIVIK TARGET AIRCRAFT. Harrison, J.E.A. November, 1962.

This note describes measurements of apparent radar glint and range performance made by using AI Mk.18 and AI Mk.23B radars against a Jindivik carrying various arrangements of Luneberg lenses. Although the results are few and statistically somewhat dissatisfying, they agree sufficiently closely with theory to make them worth while publishing.

Generally, a Luneberg lens of 20 sq. m. equivalent echoing area allows AI Mk.18 and AI Mk.23B radars to lock-on at about 20 miles, which is comparable with lock-on ranges achieved on Canberra aircraft viewed from dead astern.

SECRET (Over)

SECRET

Technical Note No. I.R.13
Royal Aircraft Establishment, Aberporth

535.317.1:
621.396.963[A1](94)
Jindivik

THE USE OF LUNEBERG LENSES FOR RADAR ENHANCEMENT OF THE JINDIVIK TARGET AIRCRAFT. Harrison, J.E.A. November, 1962.

This note describes measurements of apparent radar glint and range performance made by using AI Mk.18 and AI Mk.23B radars against a Jindivik carrying various arrangements of Luneberg lenses. Although the results are few and statistically somewhat dissatisfying, they agree sufficiently closely with theory to make them worth while publishing.

Generally, a Luneberg lens of 20 sq. m. equivalent echoing area allows AI Mk.18 and AI Mk.23B radars to lock-on at about 20 miles, which is comparable with lock-on ranges achieved on Canberra aircraft viewed from dead astern.

SECRET (Over)

SECRET

Technical Note No. I.R.13
Royal Aircraft Establishment, Aberporth

535.317.1:
621.396.963[A1](94)
Jindivik

THE USE OF LUNEBERG LENSES FOR RADAR ENHANCEMENT OF THE JINDIVIK TARGET AIRCRAFT. Harrison, J.E.A. November, 1962.

This note describes measurements of apparent radar glint and range performance made by using AI Mk.18 and AI Mk.23B radars against a Jindivik carrying various arrangements of Luneberg lenses. Although the results are few and statistically somewhat dissatisfying, they agree sufficiently closely with theory to make them worth while publishing.

Generally, a Luneberg lens of 20 sq. m. equivalent echoing area allows AI Mk.18 and AI Mk.23B radars to lock-on at about 20 miles, which is comparable with lock-on ranges achieved on Canberra aircraft viewed from dead astern.

SECRET (Over)

SECRET

Technical Note No. I.R.13
Royal Aircraft Establishment, Aberporth

535.317.1:
621.396.963[A1](94)
Jindivik

THE USE OF LUNEBERG LENSES FOR RADAR ENHANCEMENT OF THE JINDIVIK TARGET AIRCRAFT. Harrison, J.E.A. November, 1962.

This note describes measurements of apparent radar glint and range performance made by using AI Mk.18 and AI Mk.23B radars against a Jindivik carrying various arrangements of Luneberg lenses. Although the results are few and statistically somewhat dissatisfying, they agree sufficiently closely with theory to make them worth while publishing.

Generally, a Luneberg lens of 20 sq. m. equivalent echoing area allows AI Mk.18 and AI Mk.23B radars to lock-on at about 20 miles, which is comparable with lock-on ranges achieved on Canberra aircraft viewed from dead astern.

SECRET (Over)

SECRET

The angle noise produced by two 12" lenses or a 10" and a 12" lens mounted on the wingtips of a Jindivik appears comparable with that produced by a Canberra at similar ranges.

SECRET

SECRET

The angle noise produced by two 12" lenses or a 10" and a 12" lens mounted on the wingtips of a Jindivik appears comparable with that produced by a Canberra at similar ranges.

SECRET

SECRET

The angle noise produced by two 12" lenses or a 10" and a 12" lens mounted on the wingtips of a Jindivik appears comparable with that produced by a Canberra at similar ranges.

SECRET

SECRET

The angle noise produced by two 12" lenses or a 10" and a 12" lens mounted on the wingtips of a Jindivik appears comparable with that produced by a Canberra at similar ranges.

SECRET

[dstl]

Information Centre
Knowledge Services
[dstl] *Porton Down,*
Salisbury
Wilts
SP4 0JQ
22060-6218
Tel 01980-613753
Fax 01980-613970

Defense Technical Information Center (DTIC)
8725 John J. Kingman Road, Suit 0944
Fort Belvoir, VA 22060-6218
U.S.A.

AD#: AD337278

Date of Search: 12 February 2009

Record Summary: AVIA 6/23869
Use of Luneberg lenses for radar enhancement of JINDVIK target aircraft
Former reference (Department): Technical Note No Ir13
Held by The National Archives, Kew

This document is now available at the National Archives, Kew, Surrey, United Kingdom.

DTIC has checked the National Archives Catalogue website (http://www.nationalarchives.gov.uk) and found the document is available and releasable to the public.

Access to UK public records is governed by statute, namely the Public Records Act, 1958, and the Public Records Act, 1967.
The document has been released under the 30 year rule.
(The vast majority of records selected for permanent preservation are made available to the public when they are 30 years old. This is commonly referred to as the 30 year rule and was established by the Public Records Act of 1967).

This document may be treated as <u>UNLIMITED</u>.